Free Radical Biology and Medicine 143 (2019) 115–126

Contents lists available at ScienceDirect

Free Radical Biology and Medicine

journal homepage: www.elsevier.com/locate/freeradbiomed

Original article

Alcohol promotes waste clearance in the CNS via brain vascular reactivity

Yiming Cheng[a], Xinglei Liu[b], Xiaotang Ma[a], Ricardo Garcia[a], Kevin Belfield[b], James Haorah[a,*]

[a] Laboratory of Neurovascular Inflammation and Neurodegeneration, Department of Biomedical Engineering, Center for Injury Bio Mechanics, Materials and Medicine, New Jersey Institute of Technology, Newark, NJ, 07102, United States

[b] Department of Chemistry and Environmental Science, College of Science and Liberal Arts, New Jersey Institute of Technology, 323 Martin Luther King, Jr., Blvd., Newark, NJ, 07102, United States

ARTICLE INFO

Keywords:
CNS clearance
CSF
Perivascular space
Alcohol
eNOS

ABSTRACT

The efficient clearance of the interstitial waste metabolites is essential for the normal maintenance of brain homeostasis. The brain lacks the lymphatic clearance system. Thus, the drainage of waste metabolites in the brain is dependent on a slow flow of cerebrospinal fluid (CSF) system. Glymphatic system claims the direct bulk flow transport of small size water-soluble waste metabolites into to the perivenous space by aquaporin-4 water channels of the astrocyte end-feet, but it did not address the diffusive clearance of large size waste metabolites. Here, we addressed the clearance mechanisms of large size waste metabolites from interstitial fluid to perivascular space as well as from CSF subarachnoid into perivascular space via the paravascular drainage. A low dose ethanol acting as a potent vasodilator promotes the dynamic clearance of waste metabolites through this perivascular-perivenous drainage path. We observed that ethanol-induced increased in vascular endothelial and smooth muscle cell reactivity regulated the enhanced clearance of metabolites. Here, activation of endothelial specific nitric oxide synthase (eNOS) by ethanol and generation of vasodilator nitric oxide mediates the interactive reactivity of endothelial-smooth muscle cells and subsequent diffusion of the CNS waste metabolites towards perivascular space. Detection of tracer dye (waste metabolite) in the perivenous space and in the blood samples further confirmed the improved clearance of waste metabolites through this unraveled interstitial-perivascular-perivenous clearance path. Our results suggest that alcohol intake at low-dose levels may promote clearance of neurological disease associated entangled proteins.

1. Introduction

Efficient clearance of interstitial fluid (ISF) waste metabolites by cerebrospinal fluid (CSF) flow is essential for normal healthy maintenance of brain homeostasis, because unlike most tissue organs the brain lacks a lymphatic system. The classical view of the CNS clearance system is that the interstitial fluid (ISF) contains the extracellular and intracellular waste metabolites that are drained into choroid plexus [1], from here CSF flows into subarachnoid space (SA) through the median and lateral apertures. CSF is then exchanged into dural sagittal sinuses via a restricted granulation known as subarachnoid microvilli, then the sagittal sinuses, merged at the confluence of sinuses, are drained into nasal or cervical lymphatic vessels [2–4]. Johnston et al. (2010) showed this path by filling the subarachnoid compartment of seven different species, from small rodents to humans, with yellow microfil CSF tracer dyes to trace the drainage path of CSF into nasal lymphatics [5]. They found that microfil was observed primarily in the subarachnoid space around the olfactory bulbs and cribriform plate. The contrast agent followed the olfactory nerves and entered extensive lymphatic networks in the submucosa associated with the olfactory and respiratory epithelium.

Recently, Louveau et al. (2015) and Aspelund et al. (2015) have shown the existence of dura associated lymphatic vascular system in the brain's meninges whole-mount fixing the meninges still attached to the skull [6,7]. They observed distinctive expression of lymphatic endothelial cells including lymphatic vessel endothelial hyaluronan receptor 1 (Lyve-1) and vascular endothelial growth factor receptor 3 (VEGFR3) along the blood vessels of superior sagittal and transverse sinuses. The involvement of dural lymphatic vessels for the drainage of metabolites in dural venous sinus was shown by injecting tracers into the CSF of animals and by detecting the tracers in the lumen of Lyve-1-expressing vessels and in the deep cervical lymph nodes [6]. It was further confirmed that there was a significant reduction of tracers in Lyve-1-expressing vessels and a complete absence of tracers in the cervical lymph nodes of transgenic mice deprived of lymphatic vessels [7]. Since anatomical sites of lymphatic vessels were strictly localized

* Corresponding author.
E-mail address: james.haorah@njit.edu (J. Haorah).

https://doi.org/10.1016/j.freeradbiomed.2019.07.029
Received 20 May 2019; Received in revised form 26 July 2019; Accepted 26 July 2019
Available online 27 July 2019
0891-5849/

in brain dura meninges [6–8], as such transport of soluble waste metabolites into lymphatic vessels would be dependent on CSF subarachnoid circulation. Notably, the exchange of waste metabolites from subarachnoid to superior sagittal venous sinus is valid only for water-soluble small size metabolites because of granulated subarachnoid microvilli barriers. Thus, dural lymphatic vessels, also known as meningeal lymphatic clearance system may not clear large size waste metabolites.

The recently discovered glymphatic system showed a molecular size dependent clearance profile of fluorescent dye tracers in the CNS, when tracers were injected through intracisterna magna [9]. The small size tracer (Texas Red, 3 kDa) directly entered the interstitial space and influx into the perivascular space along penetrating arterioles. The clearance of this small size tracer from perivascular space into central deep veins and lateral-ventral caudal rhinal veins is facilitated by aquaporin-4 (AQP4) water channel of a highly-polarized astrocytic end feet. Such an AQP4 facilitated exchange between CSF and ISF is restricted to small size waste metabolites because the medium size tracer (Ovalbumin, 647 kDa) gets accumulated at perivascular space within 3 h of injection. The tracer then slowly penetrated into the basement membranes of parenchymal capillaries and perivascular space of large caliber draining veins, suggesting a capillary-venous drainage route. In contrast, a large size tracer (FITC, 2000 kDa) was found to be aggregated at the perivascular space, lacking a distinct clearance path [9]. Injection of radiolabeled amyloid β1–40 (Aβ, a small peptide) into mouse striatum was rapidly cleared through the glymphatic pathway since the clearance was significantly diminished in AQP4 deficiency transgenic mice [9]. This further implicates the importance of glymphatic system clearance in neurological disease, like Alzheimer's disease [9–12], even though glymphatic system did not account for the clearance of such large size waste metabolites in the CNS.

However, the reproducibility of the accredited bulk flow transport mechanism of glymphatic hypothesis has been questioned by a number of most recent verification studies. These investigations concluded that clearance of waste metabolites from the brain is more of a diffusion rather than bulk flow convective transport, based on the metabolites molecular size [13,14]. In support of this argument, a model of diffusive and convective transport in brain extracellular space stated that diffusion alone size [15] or combined effects of diffusion and macroscopic fluid motion [16] is adequate to account for transport of waste metabolites in brain parenchyma rather than bulk flow alone. The later appears to be a more reconcile argument for such conflicting experimental observations, notably the transport of solutes in opposite directions in the perivascular space. This is in parallel with the findings that cyclic changes in arterial pressure produces mixing or flow in opposite directions in different spaces of the arterial wall [17]. In this case, convection can assist the movement into and out of the cortex without necessarily producing the net flow of fluid into the cortex as required by glymphatic system. Furthermore, the diffusive molecular flow along the peri-arterial sheaths into subarachnoid CSF [18], and the diffusive drainage of waste metabolites from brain parenchyma into the basement membrane of capillaries [19] argued against the glymphatic hypothesis.

The fact is that large size waste metabolites like tauopathy, prion-like proteinopathies, cerebral amyloid angiopathy, and Aβ proteins are seen accumulated around the perivascular space in brain tissue from neurological diseases [20–22]. Such observations suggest that large size waste metabolites are not cleared by CSF, glymphatic, or meningeal lymphatic systems. Here, we address the fundamental questions of what dynamic force specifically drives the movement of these waste metabolites towards perivascular space, and can we strategize to enhance the clearance of these waste metabolites from perivascular space into the circulation? It has been shown that the blood-brain barrier (BBB) trans-vascular clearance from brain to blood provides functionally a major pathway for elimination of different waste metabolic products from brain into the circulation including amyloid-beta, which is believed to account for > 80% of amyloid-beta clearance under physiological conditions [23–25]. Thus, uncovering the mechanisms of moving the waste metabolites towards perivascular space and the clearance of waste metabolites from perivascular space into the circulation should have significant clinical impact for possible prevention of many neurological diseases. We hypothesize that increasing the reactivity of brain arterial endothelial and smooth muscle cell function by low dose ethanol can enhance the dynamic diffusion of water-insoluble large size CSF/interstitial metabolites into perivascular space and subsequent clearance into the circulation. Here we test the idea that activation of brain endothelial specific nitric oxide synthase (eNOS) by low dose ethanol produces potent vasodilator nitric oxide that can diffuse readily into the underlying SMCs to cause arterial vessel dilation through intracellular calcium signaling. The rationale is that activation of eNOS by low concentration of ethanol elevates physiological NO levels and augments endothelial-SMCs interactive reactivity [26–28]. This eNOS derived NO acts as a potent protective brain vascular tone and vasodilation [29].

2. Materials and methods

Reagents: Primary antibodies rabbit anti-GFAP; mouse anti-SMA, anti-eNOS, anti-beta actin were purchased from Abcam (Cambridge, MA); anti-endomucin was purchased from Invitrogen (Carlsbad, CA). All secondary Alexa Fluor conjugated antibodies were purchased from Invitrogen (Carlsbad, CA). Table 1 summarizes the details of the antibodies source, catalog numbers, and dilutions factors that were used for immunofluorescence staining and western blotting analyses. A highly stable fixable dextran-conjugated Fluorescein, 2,000,000 MW (FITC-d2000) was purchased from Thermo Fisher Scientific (Waltham, MA), Nω-Nitro-L-arginine methyl ester (L-NAME, a NOS inhibitor) was purchased from Sigma-Aldrich (St. Louis, MO).

Animals and drug concentrations: Eight-week old male Sprague-Dawley rats were purchased from Charles River Laboratory (Wilmington, MA). Animals were maintained in sterile cages under pathogen-free conditions in accordance with institutional ethical guidelines for care of laboratory animals, National Institutes of Health guidelines, and the Institutional Animal Care Use Committee, Rutgers University. Animals were randomly divided into 4 experimental groups (6 rats/group), 1) Control, 2) 5.0 mM ethanol, 3) 5.0 mM ethanol + L-NAME, and 4) L-NAME. A working concentration of 5.0 mM ethanol (EtOH, 0.230 g/kg body weight) was determined from a dose-dependent study of 0.046–0.460 g/kg body weight reconstituted in saline. Ethanol or the NOS inhibitor L-NAME (10 mg/kg body weight) constituted in saline was injected through tail vein using a 27 G needle. Detailed experimental conditions for control tracer dye bio-distribution

Table 1
Antibodies source, catalogue numbers, and dilutions factors for immunoflurescence staining and western blotting analyses.

Antibody	Marker for	Company	Catalogue #	Dilution for IHC	Dilution for WB
Anti-α-SMA	Alpha smooth muscle actin	Abcam	ab7817	1:250	1:1000
Anti-GFAP	Astrocyte	Abcam	ab7260	1:250	–
Anti-eNOS antibody	Endothelial nitric oxide synthase	Abcam	ab76198	1:250	1:1000
Anti-β-actin antibody	Beta-actin	Abcam	ab8226	–	1:2000
Anti-Endomucin	Endomucin	Invitrogen	14-5851-82	1:200	–

through cisterna magna or intracortical route of injection is described below. For group 2, ethanol was administered 15 min prior to tracer dye injection following anesthesia, while L-NAME was administered 5 min prior to ethanol and 20 min prior to tracer dye injection for group 3. For group 4, L-NAME was given 20 min prior to tracer dye injection.

Injection of Fluorescence Marker: All rats were anesthetized by intraperitoneal injection of 0.1 ml of ketamine (80–100 mg/kg) + xylazine (5–10 mg/kg) mixture using a 26-gauge needle as approved by the Panel on Euthanasia of the American Veterinary Medical Association (AVMA). Anesthetized rats were fixed in a stereotaxic frame. Then a total volume of 10 μl fluorescence tracers diluted in artificial CSF at a concentration of 5 mg/ml (0.5%) was injected via the cisterna magna at a rate of 2 μl/min over 5 min using 30-gauge needle syringe pump (Harvard Apparatus). The body temperature of animals was maintained at 37 °C with a temperature-controlled warming pad. Heart rate and respiratory rate were monitored through MouseSTAT® Pulse Oximeter & Heart Rate Monitor Module. To visualize the time-dependent movement of tracer from subarachnoid space into the brain parenchyma following cisterna magna injection, animals were perfusion fixed at 30 min, 1 h and 2 h before surgically removing the intact brain tissues. A thickness of 40 μm tissue slices were cut and mounted on a glass covered slides and tracer bio-distribution was imaged *ex-vivo* by epifluorescence microscopy.

Intracortical tracer injection: All rats were anesthetized as describes above. A total volume of 1.0 μl fluorescent labeled tracers were injected stereotactically into the brain parenchyma at a rate of 10 nl/s that controlled by a micro syringe pump (UMP3) from world precision instruments (Sarasota, FL). A 33-gauge needle was inserted via a small burr hole into the brain at the following coordinates: right parietal skull, 2.0 mm lateral from the sagittal suture and 3.0 mm caudal from the coronal suture. After needle insertion, 30 min was given to allow the needle track to swell closed. To evaluate tracer bio-distribution, animals were perfusion-fixed between 1 – 4 h after injection and tissue slices (40 μm) were subsequently imaged as describe above.

Ex-vivo fluorescence imaging: Multi-channel whole-slice montages were acquired with Leica Aperio Versa 200 digital pathology grade slide scanner. This included separate DAPI, Green and Red emission channels. Exposure levels were determined based upon uninjected control slices, then maintained constant throughout the study. Fluorescent intensities were quantified using AreaQuant software specifically designed for this imaging application (Leica Biosystems) and expressed as average fluorescence intensity/unit area. This imaging technique allows for visualization of micro-structural details and digital scanning affords the ability to image large brain regions with no loss of resolution. In order to quantify fluorescence intensities, regions of interest were manually outlined in different brain section. For each channel (green 488 nm and red 594 nm), a minimum intensity threshold value was selected to exclude any background fluorescence from our calculation. The AreaQuant algorithm then determines if the intensity value of each pixel enclosed in the outlined region exceeds the minimum intensity threshold and outputs the total area of positive stain for each brain regions, the average intensity in each channel, and the expression profile of the tracers.

Surgery for two-photon *in-vivo* imaging: Rat surgery for two-photon imaging was as described by Eyo et al. [30]. Briefly, rats were anesthetized and craniotomy (4.0 × 4.0 mm) was performed over the right parietal skull, 2.0 mm lateral from the sagittal suture and 3.0 mm caudal from the coronal suture, with the dura intact. A head plate was glued to the skull around the cranial window, and the plate was screwed into a customized stage and placed under the two-photon microscope. To visualize vasculatures, 1 ml BBB impermeable Texas Red-dextran 70 (MW 70 kDa; 1% in saline, Invitrogen) was injected through tail vein 30 min before imaging. Rats were maintained under anesthesia and body temperature was kept at 37 °C with a warming pad for the duration of imaging. Heart rate and respiratory rate were monitored as previous described.

In vivo imaging: Two-photon microscopy setting and operation were as described [31]. In brief, two-photon fluorescence microscopy (2PFM) was performed using a Bruker Ultima fluorescence microscope equipped with a Coherent Mira 900 laser source (200 fs, 76 MHz). The excitation wavelength was 860 nm for dextran-conjugated FITC and Texas Red, and the emission was collected using two external non-descanned PMT detectors (NDD) at 525–600 nm. A 20 ×, 1.0 N A. water immersion objective was employed for the 2PFM. A laser line-scan or ROI-based local excitation was used to better evaluate vessel diameter change and tracer movement over time.

Line scan: To measure vessel diameters, 9000 ms X–Y line scan was conducted orthogonal to the vessel axis in penetrating arterioles 50–100 μm below the cortical surface. A customized Matlab code was developed to extract and calculate vessel diameter over time.

Immunofluorescent staining: Immunostaining was described in previously publications [29,32]. In brief, frozen brain tissue sections (10 μm thickness) on glass slides were washed with PBS, fixed in acetone-methanol (1 : 1 v/v) fixative, blocked the cellular antigen with 3% bovine serum albumin at room temperature for 1 h in the presence of 0.4% Triton X-100 and incubated with respective primary antibodies such as rabbit anti-alpha smooth muscle actin(SMA) (1 : 250 dilution), rabbit anti-GFAP (1 : 250 dilution) and mouse anti-eNOS (1:250 dilution) for overnight at 4 °C. After washing with PBS, tissue sections were incubated for 1 h with secondary antibody: anti-rabbit-IgG Alexa fluor 594 (1:400 dilution) for GFAP and mouse-IgG Alexa fluor 594 (1:400 dilution) for SMA and eNOS. Cover slips were then mounted onto glass slides with mounting solutions containing DAPI (Invitrogen), and fluorescence microphotographs were captured by Leica Aperio Versa 200 digital pathology grade slide scanner.

Western blot: A cerebral blood vessel isolation was performed using mesh filtration to concentrate protein content that originated solely from vasculatures [33]. In brief, fresh brain tissue was homogenized on ice using pestle in HBSS solution with 1% HEPES. Whole brain homogenization was centrifuged at 2,000 × *g* for 10 min and 4,400 × *g* for 15 min (in 20% dextran) at 4 °C. Then, pellet containing vessels was re-suspended into ice-cold 1% bovine serum albumin (BSA) solution and proceed to mesh filter (20 um) for isolation. Western blot was performed as described by previous publication [34]. In brief, isolated brain vessels were lysed with CellLytic-M (Sigma) for 30 min at 4 °C, and centrifuged at 14000 × *g*. The concentrations of protein from tissue homogenates were estimated by bicinchoninic acid (BCA) method (Thermo Fisher Scientific, Rockford, IL). Protein load was 20 μg/lane in 4–15% SDS-PAGE gradient gels (Thermo Fisher Scientific). Molecular size separated proteins were then transferred onto nitrocellulose membranes, blocked with superblock (Thermo Fisher Scientific), and incubated overnight with respective primary antibody to alpha-SMA, eNOS and beta-actin (all diluted at 1:1000) at 4 °C, followed by washes and incubation with horse-radish peroxidase conjugated secondary antibodies (corresponding to primary, diluted at 1:12000) for 1 h at room temperature. Immunoreactive bands were detected by West Pico chemiluminescence substrate (Thermo Fisher Scientific). Data was quantified as arbitrary densitometry intensity units using the ImageJ software package.

Real-time NO detection: Briefly, freshly isolated brain tissues was prepared in ice-cold oxygenated (95% O_2 and 5% CO_2) artificial cerebrospinal fluid (aCSF). Coronal slice (1 mm) was prepared using brain matrices and transferred to a recovery chamber for 30 min with oxygenated aCSF at 37 °C temperature before experiment. NO was measured using free radical analyzer with a specific NO probe (TBR4100, World Precision Instruments, Sarasota, FL). The NO probe is able to polarographically measure the concentration of NO gas in solutions. The system was calibrated using different concentrations of NO donor S-Nitroso-N-acetyl-DL-penicillamine (SNAP, Cayman Chemical) to generate a standard curve. To block endogenous NO, oxygenated aCSF containing 1 mM L-NAME was added to tissue 30 min prior experiments. Probe was positioned ~1 mm above tissue surface using a

micromanipulator (World Precision Instruments, Sarasota, FL) and baseline of NO release was recorded prior EtOH treatment. Tissue was then treated with 5 mM EtOH (in aCSF) and subsequently with 1 mM L-NAME (in aCSF). NO concentration was recorded using NO probe as described at the same time. Experiment was simultaneously performed with control from the same tissue source to exclude experimental drift in NO release unrelated to the study.

Plasma fluorescence intensity: Whole blood was collected from the tail vein before sacrificing and stored in citrate-treated blood tubes (Fisher) to avoid coagulate. To extract plasma, whole blood was centrifuged at 1000 × *g* for 10 min (4 °C). Clear supernatant was carefully collected and aliquoted into small tubes. Arbitrary fluorescence intensity was determined in 96-well plate using plate reader (Molecular Devices) at 490 excitation and 525 emission wavelengths.

Data analysis: All results values are expressed as the mean ± SE, N = 6. Statistical analysis of the data was performed using SPSS 24 (IBM). In the present studies, wherever the numeric values of N are indicated, it represents the actual number of animals/samples used for that specific experiments or the actual number of experiments performed in cell culture setting, and not the number of replicates per experimental condition. Comparisons between samples were performed by ANOVA with Tukey's post-hoc tests. Differences were considered significant at $p < 0.05$.

3. Results

The present studies examined the idea that reactivity of endothelial and smooth muscle cells plays a critical role in the interstitial-perivascular-perivenous clearance of large size waste metabolites in the brain. Here we first focused on the dynamic bio-distribution of a 2000 kDa fluorescent dye representing large size waste metabolites following two different routes of injection, through cisterna magna and direct intracranial cortical injection. Cisterna magna route directly deposits the tracer into the C3 region of CSF-subarachnoid flow, while deposition of tracer dye into the intracranial cortical region move through the interstitial space. Stimulation of brain arterial endothelial and smooth muscle cells reactivity by low dose ethanol was correlated to increase clearance of waste metabolite through interstitial-perivascular-perivenous space. We observed that reactive vascular endothelial-smooth muscle cell dilation and contraction regulates the diffusion and clearance of waste metabolites via the interstitial-perivascular-perivenous path. The clearance path is supported by our present findings.

Injection of FITC-d2000 into C3 region of CSF flow accumulates in perivascular space via the subarachnoid-paravascular movement. To evaluate the movement pattern of large size waste metabolites in the brain, we first injected FITC-d2000 (MW: 2000 kDa) directly into the CSF flow via cisterna magna which bypass the interstitial movement. This large size fluorescence tracer represents large size waste metabolite. We then evaluated the bio-distribution of tracer in the brain at different time points. We observed that a direct deposition of tracer into the C3 region of CSF-subarachnoid flow and penetrated into the perivascular space via the paravascular route time-dependently. For example, in less than 30 min after intracistertna magna injection, the subarachnoid (SAS) was filled with fluorescence tracer, but very little tracer penetrated in less than 0.5 mm depth of paravascular area from SAS (Fig. 1A). But after 60 min, more tracer was observed penetrating deep into brain perivascular space (Fig. 1B – C). The magnified imaging data from Fig. 1D – F showed the biodistribution of aggregated tracer along the different segmental branches of arterial vessel. These data suggest that waste metabolites from CSF flow can move into perivascular space through subarachnoid-paravascular drainage path.

We then evaluated the exact location of the tracer in perivascular space. The arteriole perivascular space consists of endothelial cells, pericytes, and smooth muscle cells including basement membrane proteins that are ensheathed by astrocytic end-feet from the brain side. The capillary perivascular space will contain all cellular components like in arteriole but there is absence of smooth muscle cells. Co-localization of this tracer with immunostaining of perivascular cellular markers indicated that the waste metabolite tracer was found to be entrapped in between astrocytes (Fig. 2A, GFAP) particularly at the astrocytic end-feet (Fig. 2 B & C) and vascular smooth muscle cells (Fig. 2D – G) as indicated by colocalization of alpha-SMA and tracer. We also observed that the waste metabolite tracer did not readily cross the blood vessel but aggregated around perivasculature at early time point as shown in Fig. 2E – G. These observations seen in immunostaining colocalization studies were further confirmed by multiphoton imaging techniques (Fig. 2H, H1, H2 & H3; Green: FITC-d2000, CSF tracers; Red: Texas red-d70, label vasculatures).

Intracranial cortical injection of FITC-d2000 reaches the perivascular space prior to subarachnoid clearance path. In contrast to deposition of waste metabolites directly into the CSF flow through cisterna magna injection, we also injected a FITC-d2000 tracer directly into brain interstitial space at the depth of 0.5 mm in the right cortical surface, 2.0 mm lateral to sagittal suture and 3.0 mm away from caudal coronal suture at different time points. The rationale was to determine if waste metabolites can diffuse directly into the perivascular space from site of production (parenchyma) or the route of translocation would follow the path of CSF flow via subarachnoid-paravascular clearance. We found that tracers started to diffuse directly into para-and peri-vascular space from interstitial space after 60 min of cortical injection, as indicated by Texas red-d70 labeled for vasculatures and FITC-d2000 Green representing large size waste metabolites (Fig. 3B – D). At this time point, no tracers were detected at subarachnoid space through this route of injection (Fig. 3A), indicating that waste metabolites can move directly into PVS via the interstitial diffusion. There was more accumulation of tracer in the perivascular space at longer time points of 240 min (Fig. 3E – F). This cumulative aggregation of tracer in the PVS was from interstitial movement and dynamic translocation of CSF flow because subarachnoid space was also filled with tracer at this later time point. Co-localization of tracer and vascular smooth muscle marker (alpha-SMA) immunostaining revealed that most of the tracer was arterial and capillary structures (Fig. 3G – H).

Evaluation of the putative mechanisms of tracer movement towards perivascular space. We then evaluated the putative mechanism of dynamic waste metabolites movement towards PVS that could be associated with clearance path. Based on previous findings [35-37,19] [19,35–37], we rationalized that increase in arterial vessel dilative reactivity by low-dose alcohol may regulate the movement of waste metabolites towards PVS. The justification was that low dose alcohol was known to enhance vessel dilation through nitric oxide (NO) production in endothelial cells [38]. As such, we first established the dose-response of ethanol concentrations from 2 – 10 mM on the tracer movement from CSF to perivascular space. We determined 5 mM ethanol gave the maximal biodistribution of tracer and this optimal working concentration is approximately equivalent of 0.02% blood alcohol level, which is about 4–5 times lower than the legal limit of 0.08–1.0% blood alcohol level. We observed that low dose of 5 mM ethanol injection into rat via the tail significantly ($p < 0.05$) enhanced the movement of the 2000 kDa FITC tracer from CSF to PVS compared with control (Fig. 4A). Three different regions of brain slices were selected according to rat brain atlas map (Fig. 4A), and we observed a similar trend of increased distribution of tracer by ethanol in all the three different brain regions. However, this stimulating effect of ethanol was reversed by nitric oxide synthase inhibitor L-NAME, indicating that low dose ethanol increased the movement of tracer through NOS mediated NO production.

Thus, among all isoforms of NOS, we evaluated the effects of 5.0 mM ethanol on qualitative and quantitative levels of endothelial specific eNOS, and subsequent production of NO levels in brain tissues. This biological marker was examined to validate the idea that low dose ethanol enhanced the movement of waste metabolites along the

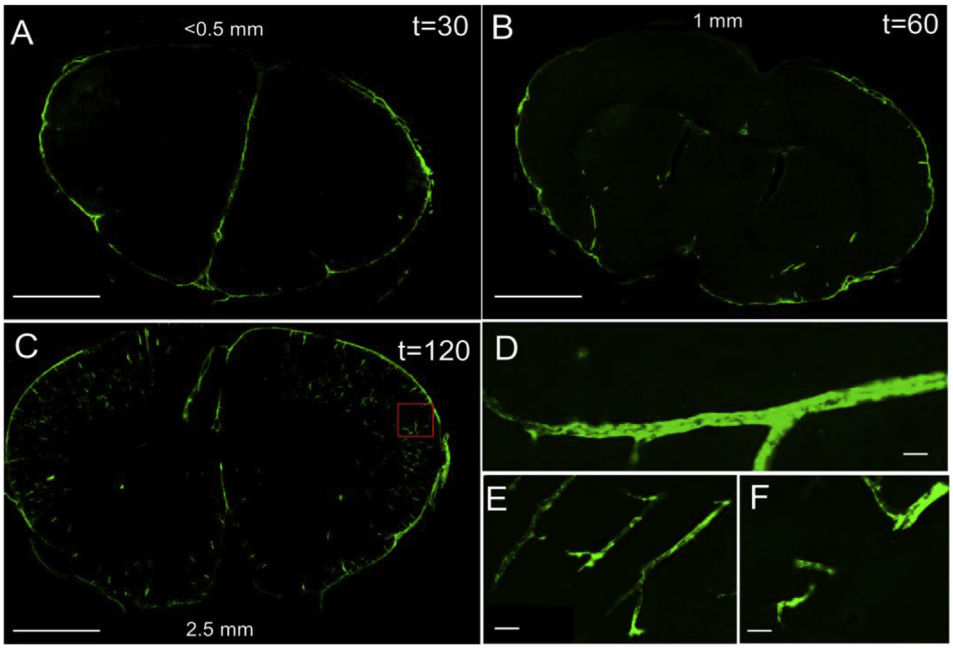

Fig. 1. Tracer bio-distribution after cisterna magna injection at 30, 60, and 120 min [A-C] data indicated that tracer was firstly filled in SAS (t < 30min), and subsequently penetrated into brain along vasculatures. [D-F] details the magnified view of vasculatures in the boxed in C. Data are representative of N = 6 animals. Scale bar: [A, B and C] 3 mm; [D, E and F]: 50 μm.

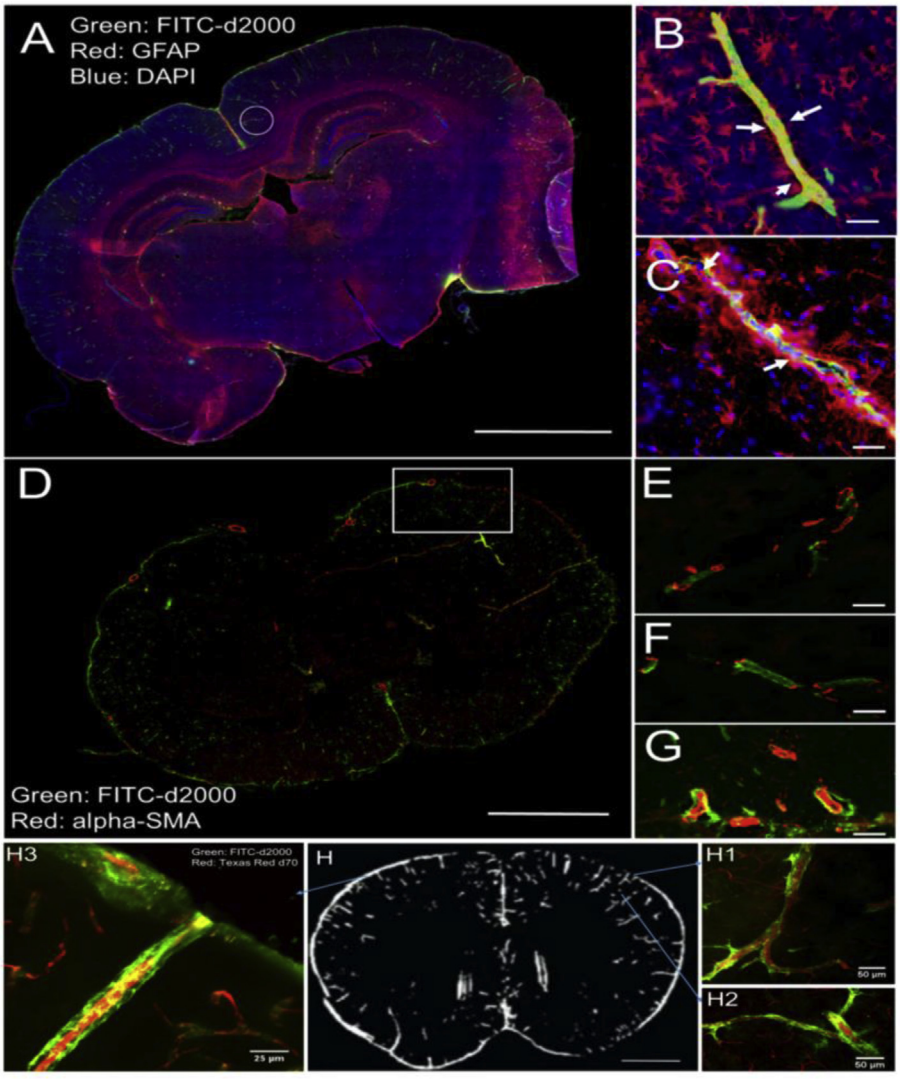

Fig. 2. Co-localization of FITC-d2000 after cisterna magna injection with astrocyte marker (GFAP) and vascular smooth muscle marker (alpha-SMA) revealed location of tracers relative to vasculatures. [A]: Co-localization of tracer (FITC-d2000, 120 min after cisterna magna injection) and astrocytes (GFAP). [B and C]: Detail views revealed that tracers were wrapped by astrocytic end-feet (white arrows). [D] Co-localization of tracer (FITC-d2000, 120 min after cisterna magna injection) and smooth muscle cells (alpha-SMA). [E – G]: Detail views on right revealed that tracers were outside smooth muscle layer, not in vessel lumen. [H]: Two-photon scanning of tracer bio-distribution (Green: FITC-d2000; Red: Texas-Red d70). Animals were injected with two types of tracers: FITC (green) was delivered through cisterna magna; Texas-Red (red) was injected through tail vein to label vasculatures. 2 h were allowed before sacrificing. [H] indicated location of vessel segments that presented in H1, H2 and H3. Data suggested that after cisterna magna injection, tracers aggregated along vasculatures. Data was representation of N = 6 animals. Scale bar: [A and D]: 3 mm; [B and C]: 100 μm; [E, F and G]; [H]: 3 mm; [H1 and H2]: 50 μm; [H3]: 25 μm. (For interpretation of the references to colour in this figure legend, the reader is referred to the Web version of this article.)

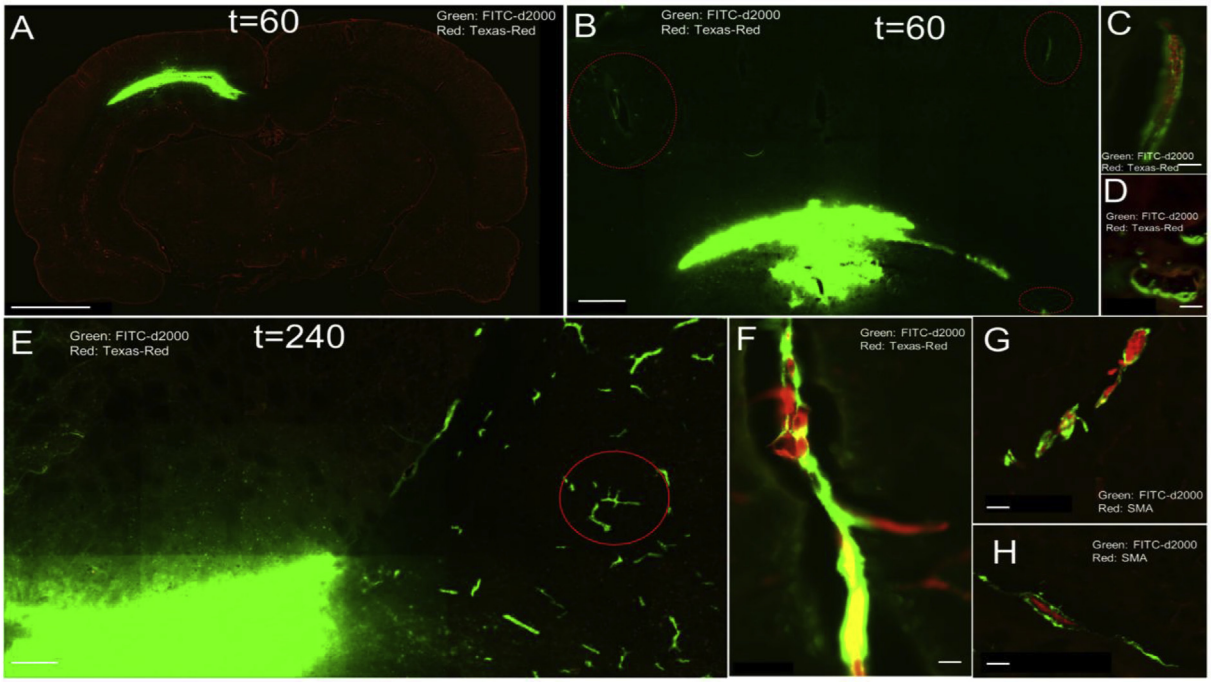

Fig. 3. Intracortical deposition of FITC-d2000 (green) directly into cortex (0.5 mm below cortical surface) allow us to track the time-dependent diffusion of tracer along the perivascular space marked by vessel marker Texas-Red d70 injected through the tail vein. 45 μm brain slices on glass slides were subjected to fluorescence microscope. [A, B, and E] indicate the time-dependent location of tracer. Small traces of tracers were already translocated from site of injection to the perivascular space before reaching to CSF, indicated by the absence of fluorescence in SAS. More tracers were found to move at longer time (E). Detail view in [C, D, F] suggested that the accumulation of tracers at PVS. [G and H]: co-localization of tracer (green) with smooth muscle actin (red) indicated that these vessels were arterials due to the presence of smooth muscle cell. Data are representative of N = 6 animals. Scale bar: A: 1 mm; B and E: 300 μm; C, D, F and G: 50 μm; H, I and J: 30 μm. (For interpretation of the references to colour in this figure legend, the reader is referred to the Web version of this article.)

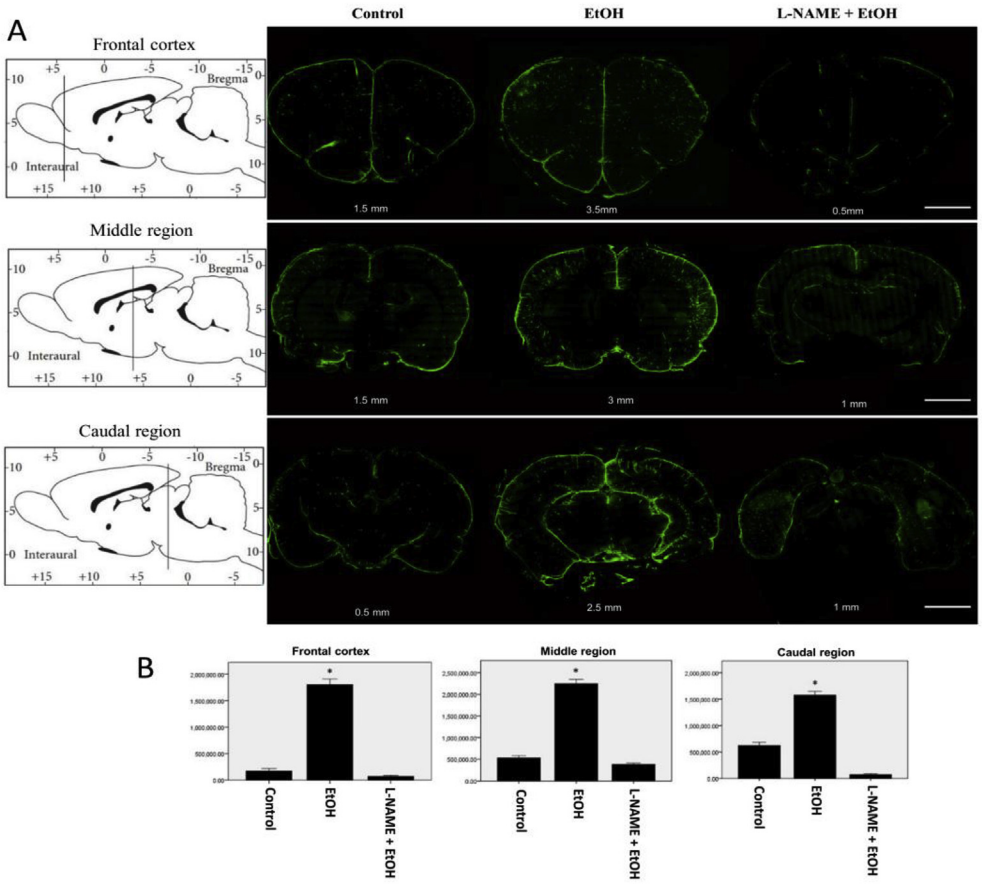

Fig. 4. [A] Bio-distribution of tracer at 2 h after cisterna magna injection in control, 5 mM EtOH, and L-NAME + 5 mM EtOH. Coordination of brain coronal tissue slices (45 μm) are shown according to rat brain map in three different locations, where bio-distribution of tracer was imaged in the whole brain section. [B] The quantity of tracer distribution in brain was calculated as mean fluorescence intensity on each slide (from N = 6 animals, 10–15 slices were taken from each animal, ± SEM). Data indicated that alcohol significantly increased the biodistribution of tracer and vascular reactivity, while NOS inhibitor L-NAME reversed the effect compared with control ($^*p < 0.05$). Scale bar: 2 mm.

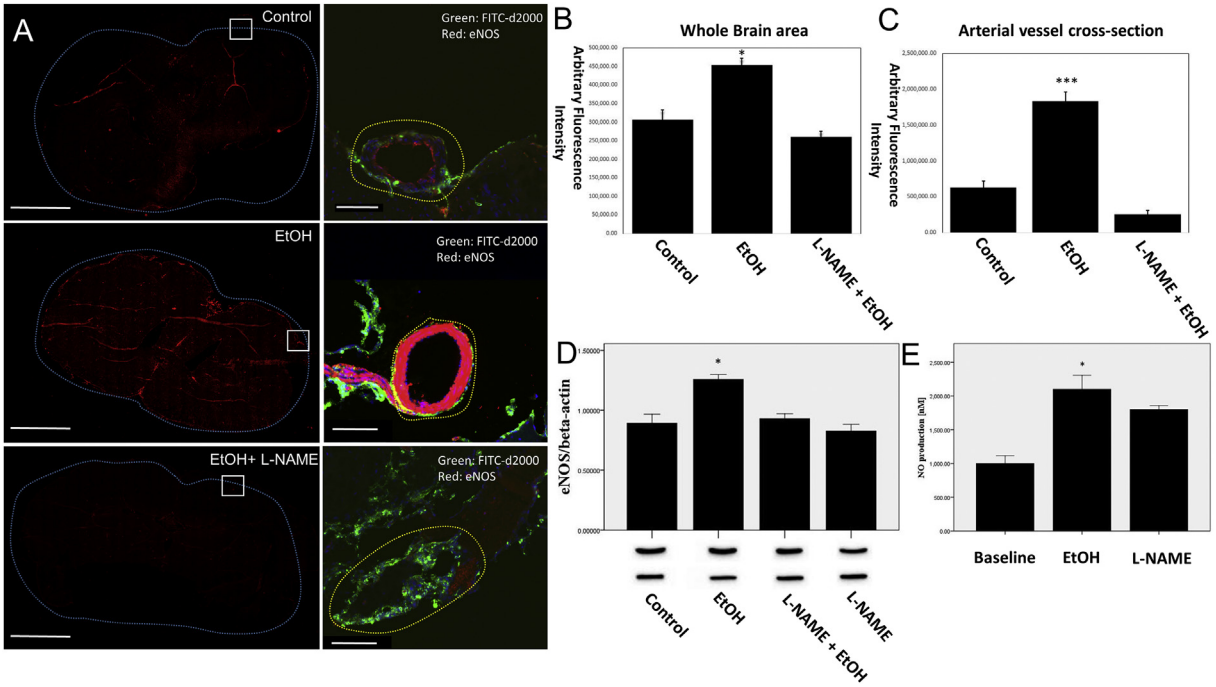

Fig. 5. Induction of eNOS by low dose ethanol produces endothelial derived nitric oxide. [A] Left: Colocalization of eNOS (red) and tracer (green) in whole brain tissue slice. Right: detailed view in boxed area. Data indicated that eNOS was elevated by EtOH. (N = 6 animals, 10–15 slices per animal). Scale bar: Left: 3 mm; Right: 50 μm. Fluorescence intensity quantification of eNOS was calculated as mean fluorescence intensity on each slide (from N = 6 animals, 10–15 slices were taken from each animal, +SEM) and presented as bar graphs, [B] whole brain scanning and [C]arterial vessel cross-section. [D] Western blot analysis of eNOS levels in different experiment conditions. Data was analyzed using image J to obtain arbitrary densitometry intensity units. Three replicates were done for each animal sample from N = 6 animals. Bar graphs data were quantified from the ratio of eNOS to that of β-actin bands, and expressed as mean ± SEM. [E] Real-time NO production in live rat brain tissue (1 mm) by Free Radical Analyzer, where NO production was simultaneously monitored. Bar graphs show the average NO concentration under each condition, and expressed as mean ± SEM. The asterisk indicates the statistical significance (*$p < 0.05$ in EtOH compare with control. (For interpretation of the references to colour in this figure legend, the reader is referred to the Web version of this article.)

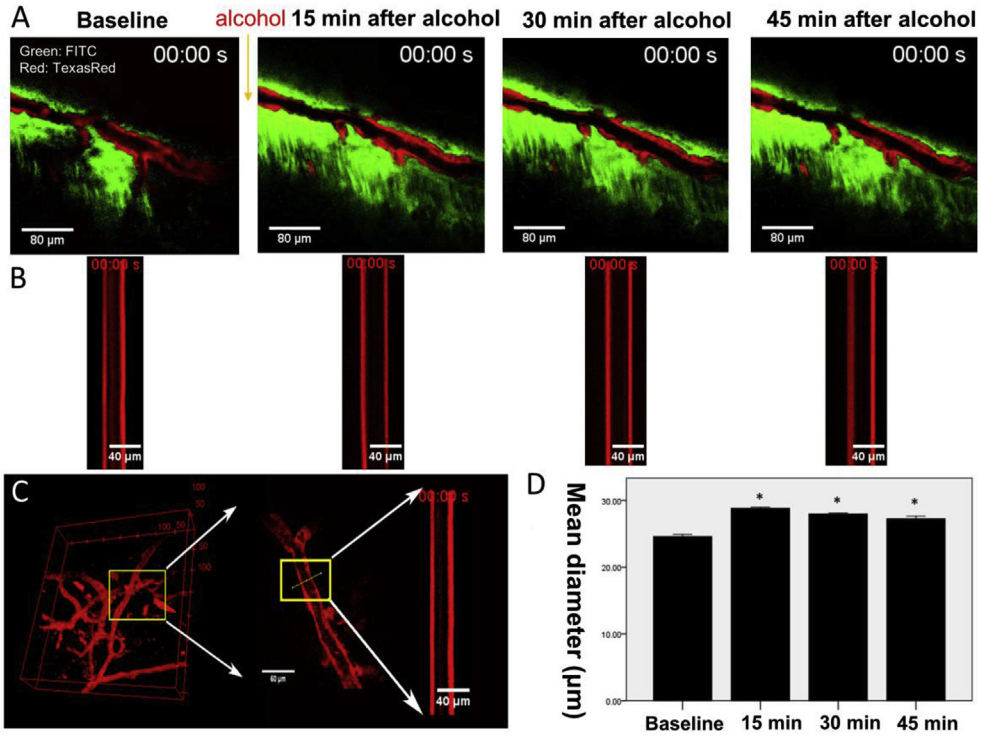

Fig. 6. Low dose alcohol enhances dynamic vessel dilation: [A] Time-lapse in vivo two-photon imaging of florescent tracer (green, injected via intracisterna) and vessel marker Texas-Red (injected via tail vein) showed the time-dependent aggregation of tracer in perivascular space in 50–100 μm below cortical surface. [B] Dynamic imaging of changes in vessel diameter over time (N = 3) before and after exposure to 5 mM ethanol at different time lapse. [C] Left: Cerebral was visualization of cerebral vasculature by two-photon imaging after intravenous tail vein injection of Texas Red-d70 showing penetrating arteriole in box (25 μm in diameter). Right: Selected area for X-T line scan to examine the changes in vessel dimeter, which was analyzed by customized Matlab at different time lapse. [D] Calculated changes in vessel dimeter, wherein baseline was collected before alcohol exposure. A 9000 ms epoch line scan was applied every 15 min to determine the changes in vessel diameter, which is shown in bar graphs. Two-way ANOVA with tukey's post-hoc test show the statistical significance *$p < 0.05$ compared with baseline, expressed as mean ± SEM, N = 3. (For interpretation of the references to colour in this figure legend, the reader is referred to the Web version of this article.)

perivasculature through NO induced vessel dilative pathway. Interestingly, immunostaining revealed a huge increase of eNOS induction by low dose alcohol group (Fig. 5A). This qualitative data was further validated by quantification of eNOS immunoreactive fluorescence intensity. Fig. 5B showed the bar graphs of whole brain scanning, and Fig. 5C presented the the bar graphs of eNOS immunoreactive localized in arterial vessel cross-section. Our data indicated a statistically significant upregulation of eNOS by low dose EtOH in the whole brain area scanning as well as in the arterial vessel cross-section compared with control ($p < 0.05$). The fold increase in arterial vessel is much higher than that of whole brain tissue section or in the whole brain tissue homogenates as detected by Western blot analysis (Fig. 5D). This is because eNOS localization and expression is specific to arterial endothelium, however, the increase levels of eNOS in whole brain tissue section imaging and in the whole brain tissue homogenate proteins are comparable as expected. To correlate the low dose ethanol-induced eNOS activation with NO generation, we analyzed the real-time NO production in live rat brain tissue by Free Radical Analyzer (World Precision Instruments, Sarasota, FL) using a micro-sensor detector. In line with eNOS activation, low dose alcohol exposure significantly elevated the production of NO in rat brain compared with baseline (Fig. 5E). As expected, co-treatment of L-NAME not only inhibited the induction of eNOS but also the production NO level. These data collectively suggest that low dose alcohol can promote perivascular clearance of waste metabolites through eNOS-mediated NO production by increasing the cerebral arterial vessel dilations.

Low dose alcohol enhances dynamic vessel dilation: To validate the proof-of-concept that ethanol-induced arterial vessel reactivity promotes the pool of waste metabolites along the PVS, we determined dynamic dilative vessel reactivity by multiphoton imaging in live animals. We found that low dose alcohol significantly increased tracer movement towards PVS within 15 min, where the flux of tracer could be detected easily in the depth of 50–100 μm below cortical surface (Fig. 6A). This increase in tracer accumulation in the PVS in the presence of alcohol was further supported by a significant vessel dilation (Fig. 6B – C) and a significant increase in arterial vessel diameter (Fig. 6D) as revealed by two photon line scan. This alcohol-induced significant increase in arterial vessel dilation and contraction suggest the active interaction between brain endothelial cell and smooth muscle cell within the arterial cellular components via the signaling molecule eNOS-elicited NO production. Such a cross-talk between endothelial cell and smooth muscle cell is unlikely to occur in the capillary since smooth muscle cells are absent in the capillary.

We then examined the idea that generation of the alcohol-induced vasodilator NO from brain endothelial cells can readily diffuse into the underlining smooth muscle cells (SMCs) reactivity. The rationale is that elevation of physiological NO levels in endothelial cell augments the endothelial-SMCs interaction to increase arterial vessel dilation. The qualitative data from immunostaining staining of α-SMCs showed an increase reactivity in low dose alcohol group compared with controls (Fig. 7A), which was in agreement with alcohol-induced NO production by endothelial cells. In parallel with an increase α-SMCs expression, the quantitative assay by Western blot analysis validated the significant elevation of α-SMCs levels in alcohol condition compared with controls (Fig. 7B). This data suggests an active interaction between vascular endothelial cells (ECs) and smooth muscle cells through a paracrine signaling pathway in which ECs derived nitric oxide acts as the key signaling molecular messenger for vessel dilation. As a work in progress, we are currently investigating the underlying molecular mechanisms that regulate smooth muscle functional activity by alcohol for promoting ECs-α-SMCs cross-talk dilative reactivity.

Vessel dilation increases waste metabolite clearance: So far, we have shown that large size waste metabolites that are not able to diffuse across the subarachnoid (SA)-superior interface (due to the presence of SA microvilli) in CSF flow get accumulated in perivascular space in the presence of low dose alcohol. This includes the interstitial-perivascular movement of waste metabolites. The diffusion of these metabolites towards the perivascular space appeared to be regulated by alcohol mediated increase in arterial vessel contraction and dilation. We then examined whether these accumulated waste metabolites at the perivascular space will diffuse into the perivenous space across the bed of capillaries, and get exchange/efflux into the blood circulation as clearance mechanisms. Our results clearly showed an increase colocalization of the 2000 kDa FITC tracer and venule marker (endomucin) in alcohol group (Fig. 8A – B) compared with controls (Fig. 8C – D), even though the tracer aggregation in perivenous space was not as high as in perivascular space. This data suggests a limited exchange of metabolites from perivascular space to perivenous space, which indicates efflux of metabolites from perivascular/perivenous space into the blood circulation.

This led us to examine validation of tracer in blood plasma samples from different experimental conditions as a proof-of-concept. Blood samples were collected at the time of sacrifice from different experimental groups with/without L-NAME injection, and separated the plasma. The 2000 kDa FITC tracer in blood plasma samples was detected by SpectraMax Multi-Mode fluorescence microplate reader at the specific excitation (490 nm) and emission (525 nm) wavelengths. We observed a significant increase of tracer fluorescence intensity in the plasma samples in low dose alcohol group compared with controls or the alcohol plus L-NAME group (Fig. 8E), indicating that low dose alcohol promotes the waste metabolites clearance path from perivascular/perivenous space into the blood circulation. These findings suggest the existence of large size waste metabolites clearance path from perivascular or perivenous space into the blood circulation, which is regulated by alcohol-induced NO mediated cerebral vessel dilation.

4. Discussion

We discuss the findings that large size waste metabolites in the brain that are unable to clear out by the conventional CSF clearance path get diffused towards perivascular-perivenous space from the interstitial fluid and from the CSF-subarachnoid flow. Thus, there is a dynamic movement of large size waste metabolites from interstitial space and subarachnoid towards perivascular space under normal physiological condition. To mimic the large size waste metabolites, we injected a large molecular weight fluorescent tracer (2000 KD) as proof-of-concept. The rationale is that due to limitation of large molecular size [9], injection of this tracer into brain seemed to accumulate at the perivascular space instead of being eliminated through CSF clearance routes including BBB trans-vascular clearance, degradation and CSF/ISF diffusion as noted by others [36]. This physiological behavior is comparable with what have been observed in certain neurological diseases including perivascular phosphorylated tau protein disposition in cerebral amyloid angiopathy (CAA) and aggregated amyloid beta protein in Alzheimer's disease [61,62]. Thus, to trace the movement of this large size waste metabolite mimic in the CNS may be considered significantly informative as proof-of-concept, however it may not accurately substitute the clearance of amyloid beta protein in Alzheimer's disease.

We firstly showed the perivascular disposition phenomenon by the bio-distribution of large size molecular weight fluorescent tracer injection from two different routes, a direct deposition of tracer into the CSF flow by intracisterna magna injection and a direct deposit of tracer into interstitial space through intracranial cortical route. Even though the subarachnoid (SAS) was filled with fluorescence tracer within 30 min, the actual penetration of tracer into the perivascular space occurred after 60 min in intracistertna magna injection (Fig. 1A–F). In the interstitial cortical injection, the tracer diffused directly into perivascular space within 60 min (Fig. 3A–D), while the CSF flow was filled with tracer at the much later time points (Fig. 3E-F), indicating the slow clearance of large size waste metabolite from interstitial fluid to C3 choroid flexus. These data suggest that waste metabolites can diffuse

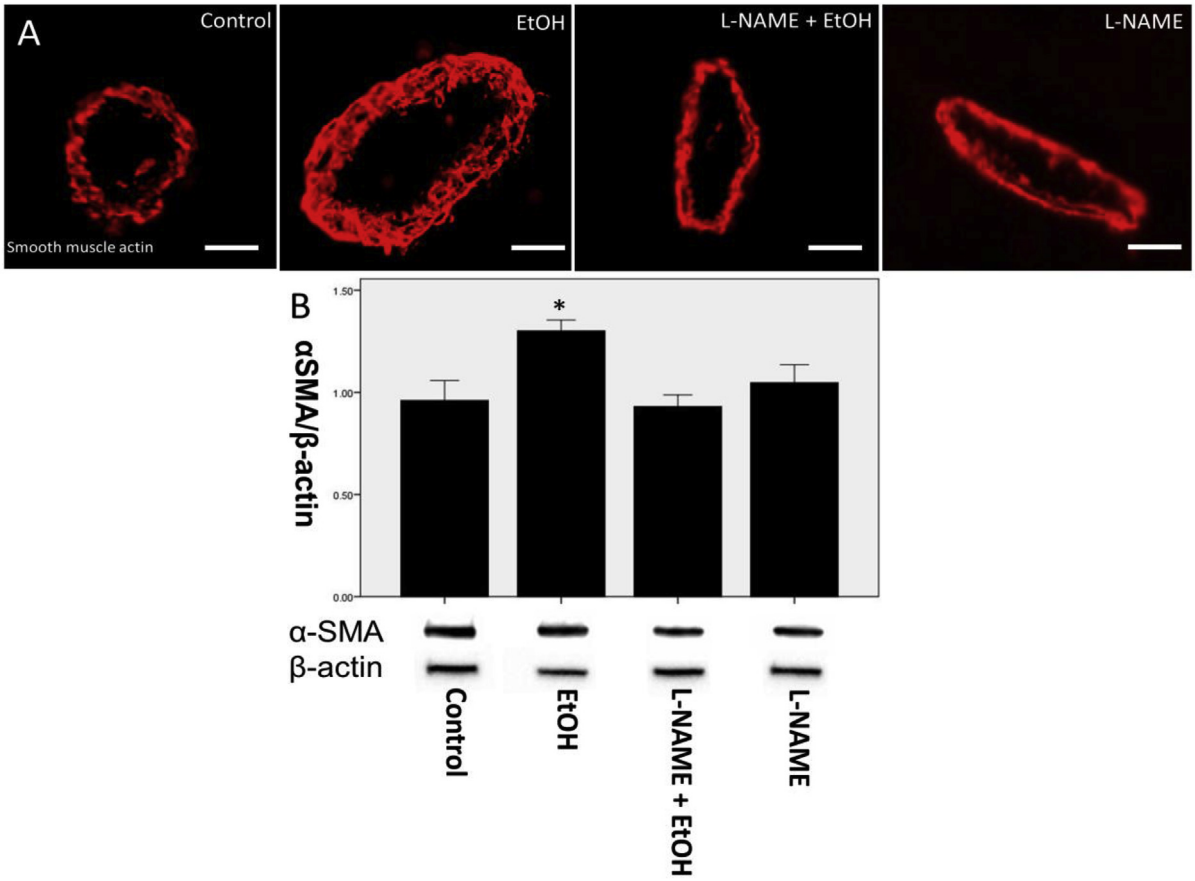

Fig. 7. [A] Shows the representative expression of brain vascular α-smooth muscle actin (αSMA, red) in whole brain tissue sections (10 μm thick) in different experiment conditions with a significant increase by ethanol exposure (N = 6 animals, 10–15 slices per animal). Scale bar: 30 μm. [B] Western blot analysis of αSMA levels in different experiment conditions. Data was analyzed by image J to obtain arbitrary densitometry intensity units. Three replicates were done for each animal per condition. Bar graphs show the quantified data that were expressed as ratio of αSMA immunoreactive bands to that of β-actin bands, with mean ± SEM. * indicates the statistical significance $p < 0.05$ compared with control or L-NAME + EtOH/L-NAME alone. (For interpretation of the references to colour in this figure legend, the reader is referred to the Web version of this article.)

directly into PVS time-dependently from interstitial fluid and from CSF-subarachnoid flow, which is regulated by endothelial-smooth muscle cell dilation. Similar alternative clearance mechanisms of direct translocation of interstitial solutes to perivascular space have been proposed in mouse model [19].

Intriguingly, our data showed that a very low level of 5.0 mM ethanol, equivalent of 0.02% blood alcohol level can enhance the dynamic movement pattern of these waste metabolites towards perivascular-perivenous space. This concentration is far below the legal limit of 0.08% blood alcohol level. In spite of alcohol being an addictive substance, the low-dose of this legalized substance is likely to improve the clearance of waste metabolites in the brain. Thereby, one drink of alcohol a day may ameliorate the progression of many neurological diseases that are originated from toxicity of non-clearance waste metabolites. Interestingly, a number of recent population-based cohort studies concluded that heavy alcohol use in chronic condition is associated with development dementia and progression of Alzheimer's disease and cerebral amyloid angiopathy [39–46], the hallmark of these neurological diseases happen to be the deposition of waste metabolites like Aβ protein, or protein prion-like proteinopathies around the perivascular space [47–49]. These cohort studies also unequivocally noted the protective effects of low dose alcohol use against the progression of dementia and AD/CAA, with unknown mechanisms. It is apparent that beneficial or destructive effects of alcohol is dependent on the duration and concentration use. In the present studies, we use low level of alcohol to understand the protective mechanisms for promoting perivascular clearance because low-moderate alcohol use is protective of vascular and cardiovascular function [50–55]. In fact, Lundgaard et al. (2018), have shown the beneficial effects of low dose alcohol and adverse effects of high dose alcohol on glymphatic function [53]. Currently we are examining the contrast effects of low dose alcohol intake and chronic use of high dose alcohol (equivalent of alcohol dependent subjects) in the context of blood-brain barrier permeability and perivascular clearance path. Our unpublished preliminary data indicated that low dose alcohol promotes perivascular waste metabolites clearance without compromising BBB integrity, unlike the long-term high dose alcohol intake.

We then addressed the underlying clearance mechanisms of the accumulated waste metabolites from perivascular or perivenous space into the blood circulation by two approaches. The exchange of waste metabolites from perivascular space to perivenous space across the bed of capillaries, and detection of waste metabolite in blood samples collected from jugular vein. Colocalization of tracer with venule marker clearly showed a significant accumulation of tracer in perivenous space of alcohol group compared with controls (Fig. 8A–D), however the tracer intensity was less than that of perivascular space (Fig. 6A). These results indicated the movement of metabolites from perivascular to perivenous space across the bed of capillary. The exchange of waste metabolites from perivascular/perivenous space into the blood circulation as the clearance path was examined by the presence of fluorescent tracer in blood plasma samples from various experimental conditions. A significant detection of tracer in the plasma samples in low dose alcohol group was markedly higher than controls or alcohol plus NOS inhibitor L-NAME groups (Fig. 8E). These data suggest that the

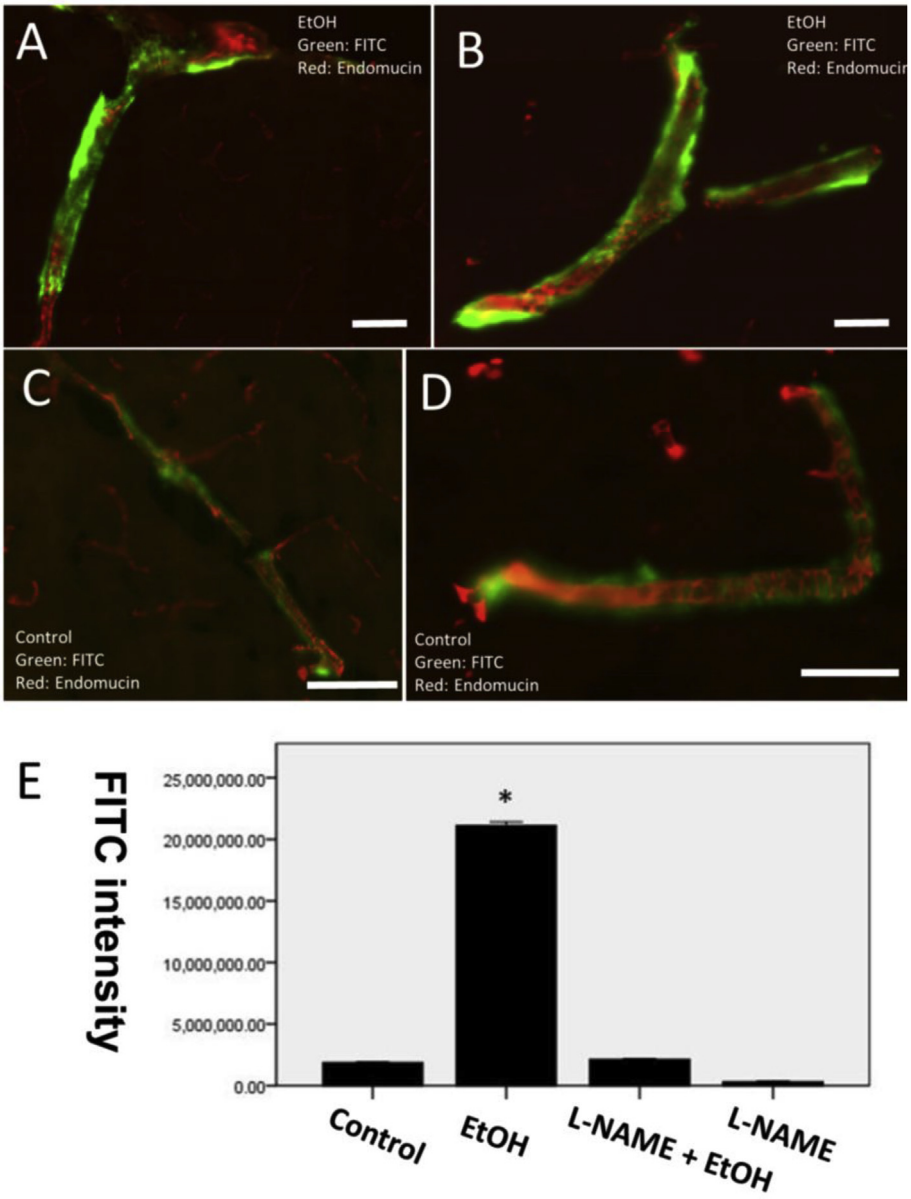

Fig. 8. Validating the diffusive exchange of waste metabolite from perivascular to perivenous space (at the bed of capillaries). [A - D] Colocalization of FITC tracer (Green) and venule marker endomucin (red) in alcohol group (A&B) compared with control (C&D), indicating an exchange of large size metabolites from perivascular space to perivenous space. [E] Detection of FITC-d2000 in blood plasma collected after 120 min cisterna magna injection from different experiment conditions, (n = 6/per group, ± SEM). One-way ANOVA and post-hoc turkey test (*$p < 0.05$, compared with control) was performed to compare difference between each group.

tracer was leaked into the circulation from perivascular/perivenous exchange because this large size waste metabolite was not permeable from subarachnoid to sagittal sinuses due to blockade by subarachnoid microvilli. The significantly low level of tracer present in NOS inhibitor plus alcohol group also suggested the direct role of alcohol-induced NO elicited perivascular/perivenous-blood circulation clearance path.

We then validated the underlying mechanisms that alcohol-elicited eNOS specific NO production promoted the cerebral arterial vessel dilation and clearance. The rationale was that NO production augmented the endothelial-smooth muscle cell reactive interactions and arterial vessel dilation. This is because low dose alcohol consumption led to an increase eNOS activity and NO production [26–28], whereas high dose chronic alcohol consumption led to detrimental consequences on vascular function [32,56,57]. In support of our hypothesis, we observed an increase reactivity of α-SMCs in low dose alcohol qualitatively and quantitative compared with controls or in the presence of NOS inhibitor (Fig. 7A-B). Our observations were in line with the findings that NO-mediated endothelial-smooth muscle cells interaction was key to arterial vessel reactive dilation [58,59], and perhaps the movement of tracer along PVS [37]. The rationale is that endothelial-derived NO generation can diffuse readily into the underlying SMCs and cause vessel dilation through a cascade of paracrine-mediated biochemical signaling events [58,60], wherein NO serves as the key signaling molecule for vessel dilation.

Apart from local level regulation of vessel dilation including response to mechanical forces (eg. shear stress) and chemical stimuli (eg. NO) as discussed above, it has been shown that vessel contraction/dilation is also dependent on neural activity coupled with sensory stimulus. For example, using whisker stimulation and cortical spreading depolarization, researchers observed microvascular diameter changes in smooth muscle covered microvessels in brain [63]. However, due to the limitation of this study scope, the current research focus was primarily on the local level regulation of regional blood vessel dilation exerted by eNOS-derived NO production in low dose alcohol. Brain

activity dependent regulation will be explored as our future scope of investigation.

In conclusion, the diffusive movement of large size waste metabolites from interstitial fluid and from CSF-subarachnoid flow into perivascular-perivenous drainage path is regulated by reactive dilation of endothelial-smooth muscle cells. We found that low dose alcohol can significantly promote these waste metabolites movement towards the perivascular-perivenous space and its clearance into the circulation. We confirmed that alcohol-elicited eNOS specific NO production regulated the cerebral arterial vessel dilation through endothelial-smooth muscle cell reactive interactions. Our present findings are expected to have far-reaching translational significance, particularly the timely clearance of entangled proteins in neurological diseases.

Competing interests

The authors have declared that no competing interests exist.

Authors contributions

YC carried out the studies, performed the acquisition data and prepared the first draft of the manuscript. XL conducted in two-photon data acquisition and processing. XM assisted YC in animal care and surgery. RG assisted in two-photon data analyzing. KB assisted in two-photon data acquisition and processing and provided important comments from his area of expertise in fluorescent probes and multiphoton fluorescence imaging. JH designed the whole project, supervised the execution of the experiments, data interpretation and prepared the manuscript. All authors read and approved the final manuscript.

Acknowledgements

This work was supported by NIH/NIAAA grant 1R21AA022734-01A1, R21 AA020370-01A1 (to JH). KDB acknowledges support from the National Science Foundation (CBET-1517273), United States.

Appendix A. Supplementary data

Supplementary data to this article can be found online at https://doi.org/10.1016/j.freeradbiomed.2019.07.029.

References

[1] L.H. Weed, Studies on cerebro-spinal fluid. No. IV : the dual source of cerebro-spinal fluid, J. Med. Res. 31 (1) (1914) 93-118.11.
[2] W.G. Bradley Jr., K.E. Kortman, B. Burgoyne, Flowing cerebrospinal fluid in normal and hydrocephalic states: appearance on MR images, Radiology 159 (3) (1986) 611–616.
[3] D.A. Feinberg, A.S. Mark, Human brain motion and cerebrospinal fluid circulation demonstrated with MR velocity imaging, Radiology 163 (3) (1987) 793–799.
[4] L.H. Weed, Studies on cerebro-spinal fluid. No.II : the theories of drainage of cerebro-spinal fluid with an analysis of the methods of investigation, J. Med. Res. 31 (1) (1914) 21–49.
[5] M. Johnston, A. Zakharov, C. Papaiconomou, G. Salmasi, D. Armstrong, Evidence of connections between cerebrospinal fluid and nasal lymphatic vessels in humans, non-human primates and other mammalian species, Cerebrospinal Fluid Res. 1 (1) (2004) 2.
[6] A. Louveau, I. Smirnov, T.J. Keyes, J.D. Eccles, S.J. Rouhani, J.D. Peske, N.C. Derecki, D. Castle, J.W. Mandell, K.S. Lee, T.H. Harris, J. Kipnis, Structural and functional features of central nervous system lymphatic vessels, Nature 523 (7560) (2015) 337–341.
[7] A. Aspelund, S. Antila, S.T. Proulx, T.V. Karlsen, S. Karaman, M. Detmar, H. Wiig, K. Alitalo, A dural lymphatic vascular system that drains brain interstitial fluid and macromolecules, J. Exp. Med. 212 (7) (2015) 991–999.
[8] D. Raper, A. Louveau, J. Kipnis, How do meningeal lymphatic vessels drain the CNS? Trends Neurosci. 39 (9) (2016) 581–586.
[9] J.J. Iliff, M. Wang, Y. Liao, B.A. Plogg, W. Peng, G.A. Gundersen, H. Benveniste, G.E. Vates, R. Deane, S.A. Goldman, E.A. Nagelhus, M. Nedergaard, A paravascular pathway facilitates CSF flow through the brain parenchyma and the clearance of interstitial solutes, including amyloid beta, Sci. Transl. Med. 4 (147) (2012) 147ra111.
[10] N.A. Jessen, A.S. Munk, I. Lundgaard, M. Nedergaard, The glymphatic system: a beginner's guide, Neurochem. Res. 40 (12) (2015) 2583–2599.
[11] J.J. Iliff, S.A. Goldman, M. Nedergaard, Implications of the discovery of brain lymphatic pathways, the Lancet, Neurology 14 (10) (2015) 977–979.
[12] J.J. Iliff, H. Lee, M. Yu, T. Feng, J. Logan, M. Nedergaard, H. Benveniste, Brain-wide pathway for waste clearance captured by contrast-enhanced MRI, J. Clin.Invest. 123 (3) (2013) 1299–1309.
[13] K.E. Holter, et al., Interstitial solute transport in 3D reconstructed neuropil occurs by diffusion rather than bulk flow, Proc. Natl. Acad. Sci. U. S. A. 114 (37) (2017) 9894–9899.
[14] A.J. Smith, et al., Test of the 'glymphatic' hypothesis demonstrates diffusive and aquaporin-4-independent solute transport in rodent brain parenchyma, Elife 6 (2017).
[15] B.J. Jin, A.J. Smith, A.S. Verkman, Spatial model of convective solute transport in brain extracellular space does not support a “glymphatic” mechanism, J. Gen. Physiol. 148 (6) (2016) 489–501.
[16] M. Asgari, D. de Zelicourt, V. Kurtcuoglu, Glymphatic solute transport does not require bulk flow, Sci. Rep. 6 (2016) 38635.
[17] S.B. Hladky, M.A. Barrand, Mechanisms of fluid movement into, through and out of the brain: evaluation of the evidence, Fluids Barriers CNS 11 (1) (2014) 26.
[18] R. Spector, S. Robert Snodgrass, C.E. Johanson, A balanced view of the cerebrospinal fluid composition and functions: focus on adult humans, Exp. Neurol. 273 (2015) 57–68.
[19] R.O. Carare, et al., Solutes, but not cells, drain from the brain parenchyma along basement membranes of capillaries and arteries: significance for cerebral amyloid angiopathy and neuroimmunology, Neuropathol. Appl. Neurobiol. 34 (2) (2008) 131–144.
[20] M. Merlini, D. Wanner, R.M. Nitsch, Tau pathology-dependent remodelling of cerebral arteries precedes Alzheimer's disease-related microvascular cerebral amyloid angiopathy, Acta Neuropathol. 131 (5) (2016) 737–752.
[21] A. Rangel, B. Race, K. Phillips, J. Striebel, N. Kurtz, B. Chesebro, Distinct patterns of spread of prion infection in brains of mice expressing anchorless or anchored forms of prion protein, Acta Neuropathol.Commun. 2 (2014) 8.
[22] C.A. Hawkes, N. Jayakody, D.A. Johnston, I. Bechmann, R.O. Carare, Failure of perivascular drainage of beta-amyloid in cerebral amyloid angiopathy, Brain Pathol. 24 (4) (2014) 396–403.
[23] R. Deane, Z. Wu, A. Sagare, J. Davis, S. Du Yan, K. Hamm, F. Xu, M. Parisi, B. LaRue, H.W. Hu, P. Spijkers, H. Guo, X. Song, P.J. Lenting, W.E. Van Nostrand, B.V. Zlokovic, LRP/amyloid beta-peptide interaction mediates differential brain efflux of Abeta isoforms, Neuron 43 (3) (2004) 333–344.
[24] M. Shibata, S. Yamada, S.R. Kumar, M. Calero, J. Bading, B. Frangione, D.M. Holtzman, C.A. Miller, D.K. Strickland, J. Ghiso, B.V. Zlokovic, Clearance of Alzheimer's amyloid-ss(1-40) peptide from brain by LDL receptor-related protein-1 at the blood-brain barrier, J. Clin.Invest. 106 (12) (2000) 1489–1499.
[25] Z. Zhao, A.P. Sagare, Q. Ma, M.R. Halliday, P. Kong, K. Kisler, E.A. Winkler, A. Ramanathan, T. Kanekiyo, G. Bu, N.C. Owens, S.V. Rege, G. Si, A. Ahuja, D. Zhu, C.A. Miller, J.A. Schneider, M. Maeda, T. Maeda, T. Sugawara, J.K. Ichida, B.V. Zlokovic, Central role for PICALM in amyloid-beta blood-brain barrier transcytosis and clearance, Nat. Neurosci. 18 (7) (2015) 978–987.
[26] C.G. Acevedo, G. Carrasco, M. Burotto, S. Rojas, I. Bravo, Ethanol inhibits L-arginine uptake and enhances NO formation in human placenta, Life Sci. 68 (26) (2001) 2893–2903.
[27] C.D. Venkov, P.R. Myers, M.A. Tanner, M. Su, D.E. Vaughan, Ethanol increases endothelial nitric oxide production through modulation of nitric oxide synthase expression, Thromb. Haemost. 81 (4) (1999) 638–642.
[28] S.S. Greenberg, J. Xie, Y. Wang, J. Kolls, J. Shellito, S. Nelson, W.R. Summer, Ethanol relaxes pulmonary artery by release of prostaglandin and nitric oxide, Alcohol (Fayetteville, N.Y.) 10 (1) (1993) 21–29.
[29] J. Haorah, N.A. Floreani, B. Knipe, Y. Persidsky, Stabilization of superoxide dismutase by acetyl-l-carnitine in human brain endothelium during alcohol exposure: novel protective approach, Free Radical Biol. Med. 51 (8) (2011) 1601–1609.
[30] U.B. Eyo, J. Peng, Regulation of Physical Microglia-Neuron Interactions by Fractalkine Signaling after Status Epilepticus vol. 3, (2016) 6.
[31] X. Yue, A.R. Morales, G.W. Githaiga, A.W. Woodward, S. Tang, J. Sawada, M. Komatsu, X. Liu, K.D. Belfield, RGD-conjugated two-photon absorbing near-IR emitting fluorescent probes for tumor vasculature imaging, Org. Biomol. Chem. 13 (43) (2015) 10716–10725.
[32] S. Alikunju, P.M. Abdul Muneer, Y. Zhang, A.M. Szlachetka, J. Haorah, The inflammatory footprints of alcohol-induced oxidative damage in neurovascular components, Brain Behav. Immun. 25 (Suppl 1) (2011) S129–S136.
[33] A.C. Boulay, B. Saubamea, X. Decleves, M. Cohen-Salmon, Purification of mouse brain vessels, J. Vis. Exp. : J. Vis. Exp. 105 (2015) e53208.
[34] J. Haorah, S.H. Ramirez, N. Floreani, S. Gorantla, B. Morsey, Y. Persidsky, Mechanism of alcohol-induced oxidative stress and neuronal injury, Free Radical Biol. Med. 45 (11) (2008) 1542–1550.
[35] E.N. Bakker, B.J. Bacskai, M. Arbel-Ornath, R. Aldea, B. Bedussi, A.W. Morris, R.O. Weller, R.O. Carare, Lymphatic clearance of the brain: perivascular, paravascular and significance for neurodegenerative diseases, Cell. Mol. Neurobiol. 36 (2) (2016) 181–194.
[36] J.M. Tarasoff-Conway, R.O. Carare, R.S. Osorio, L. Glodzik, T. Butler, E. Fieremans, L. Axel, H. Rusinek, C. Nicholson, B.V. Zlokovic, B. Frangione, K. Blennow, J. Menard, H. Zetterberg, T. Wisniewski, M.J. de Leon, Clearance systems in the brain-implications for Alzheimer disease, Nat. Rev. Neurol. 11 (8) (2015) 457–470.
[37] J.J. Iliff, M. Wang, D.M. Zeppenfeld, A. Venkataraman, B.A. Plog, Y. Liao, R. Deane, M. Nedergaard, Cerebral arterial pulsation drives paravascular CSF-interstitial fluid exchange in the murine brain, J. Neurosci. : Off. J.Soc. Neurosci. 33 (46) (2013) 18190–18199.

[38] X.S. Deng, R.A. Deitrich, Ethanol metabolism and effects: nitric oxide and its interaction, Curr. Clin. Pharmacol. 2 (2) (2007) 145–153.
[39] M. Schwarzinger, B.G. Pollock, O.S.M. Hasan, C. Dufouil, J. Rehm, QalyDays Study Group Contribution of alcohol use disorders to the burden of dementia in France 2008-13: a nationwide retrospective cohort study, 2018, Lancet Public Health 3 (2018) e124–ee32.
[40] M. Miller, D. Orwat, G. Rahimi, J. Mintzer, A retrospective, population-based cohort study of driving under the influence, Alzheimer's disease diagnosis, and survival, 2019 Apr, Int. Psychogeriatr. 31 (4) (2019) 571–577 PMID: 30303050.
[41] D. Heymann, Y. Stern, S. Cosentino, O. Tatarina-Nulman, J.N. Dorrejo, Y. Gu, The association between alcohol use and the progression of alzheimer's disease, 2016, Curr. Alzheimer Res. 13 (12) (2016) 1356–1362 PMID: 27628432 PMCID: PMC5526221.
[42] C. Avellaneda-Gómez, M. Serra Martínez, A. Rodríguez-Campello, Á. Ois, E. Cuadrado-Godia, E. Giralt-Steinhauer, R. Vivanco-Hidalgo, J. Jiménez-Conde, A. Gómez-González, P. de Ceballos Cerrajería, A. Zabalza de Torres, M. Mola-Caminal, C. Soriano-Tárraga, J. Roquer, Alcohol overuse and intracerebral hemorrhage: characteristics and long-term outcome, Eur. J. Neurol. 25 (11) (2018 Nov) 1358–1364 PMID: 29938871.
[43] J. Rehm, O.S.M. Hasan, S.E. Black, K.D. Shield, M. Schwarzinger, Alcohol use and dementia: a systematic scoping review, Alzheimer's Res. Ther. 5 (1) (2019) 11 1. PMID: 30611304 PMCID: PMC6320619.
[44] P.1 Costa, Grassi M1, iacoviello L1, zedde M1, padovani A1, pezzini A; multicenter study on cerebral haemorrhage in Italy (MUCH-Italy) investigators. Alcohol intake and the risk of intracerebral hemorrhage in the elderly: the MUCH-Italy, Neurology 91 (3) (2018 Jul 17) e227–e235 PMID: 29898970.
[45] K.J. Anstey, H.A. Mack, N. Cherbuin, Alcohol consumption as a risk factor for dementia and cognitive decline: meta-analysis of prospective studies, Am. J. Geriatr. Psychiatry 17 (2009) 542–555 PMID: 19546653.
[46] W. Xu, H. Wang, Y. Wan, C. Tan, J. Li, L. Tan, J.T. Yu, Alcohol consumption and dementia risk: a dose-response meta-analysis of prospective studies, 2017 Jan, Eur. J. Epidemiol. 32 (1) (2017) 31–42 PMID: 28097521.
[47] M. Merlini, D. Wanner, R.M. Nitsch, Tau pathology-dependent remodelling of cerebral arteries precedes Alzheimer's disease-related microvascular cerebral amyloid angiopathy, Acta Neuropathol. 131 (5) (2016) 737–752.
[48] A. Rangel, B. Race, K. Phillips, J. Striebel, N. Kurtz, B. Chesebro, Distinct patterns of spread of prion infection in brains of mice expressing anchorless or anchored forms of prion protein, Acta Neuropathol.Commun. 2 (2014) 8.
[49] C.A. Hawkes, N. Jayakody, D.A. Johnston, I. Bechmann, R.O. Carare, Failure of perivascular drainage of beta-amyloid in cerebral amyloid angiopathy, Brain Pathol. 24 (4) (2014) 396–403.
[50] C.G. Acevedo, G. Carrasco, M. Burotto, S. Rojas, I. Bravo, Ethanol inhibits L-arginine uptake and enhances NO formation in human placenta, Life Sci. 68 (26) (2001) 2893–2903.
[51] C.D. Venkov, P.R. Myers, M.A. Tanner, M. Su, D.E. Vaughan, Ethanol increases endothelial nitric oxide production through modulation of nitric oxide synthase expression, Thromb. Haemost. 81 (4) (1999) 638–642.
[52] S.S. Greenberg, J. Xie, Y. Wang, J. Kolls, J. Shellito, S. Nelson, W.R. Summer, Ethanol relaxes pulmonary artery by release of prostaglandin and nitric oxide, Alcohol 10 (1) (1993) 21–29.
[53] I. Lundgaard, W. Wang, A. Eberhardt, H.S. Vinitsky, B.C. Reeves, S. Peng, N. Lou, R. Hussain, M. Nedergaard, Beneficial effects of low alcohol exposure, but adverse effects of high alcohol intake on glymphatic function, Sci. Rep. 8 (1) (2018 Feb 2) 2246.
[54] K.J. Mukamal, et al., Roles of drinking pattern and type of alcohol consumed in coronary heart disease in men, N. Engl. J. Med. 348 (2) (2003) 109–118.
[55] P.E. Ronksley, et al., Association of alcohol consumption with selected cardiovascular disease outcomes: a systematic review and meta-analysis, BMJ 342 (2011) d671.
[56] J. Haorah, B. Knipe, S. Gorantla, J. Zheng, Y. Persidsky, Alcohol-induced blood-brain barrier dysfunction is mediated via inositol 1,4,5-triphosphate receptor (IP3R)-gated intracellular calcium release, J. Neurochem. 100 (2) (2007) 324–336.
[57] J. Haorah, D. Heilman, B. Knipe, J. Chrastil, J. Leibhart, A. Ghorpade, D.W. Miller, Y. Persidsky, Ethanol-induced activation of myosin light chain kinase leads to dysfunction of tight junctions and blood-brain barrier compromise, Alcohol Clin. Exp. Res. 29 (6) (2005) 999–1009.
[58] B. Lilly, We have contact: endothelial cell-smooth muscle cell interactions, Physiology (Bethesda, Md 29 (4) (2014) 234–241.
[59] G.A. Truskey, Endothelial cell vascular smooth muscle cell Co-culture assay for high throughput screening assays for discovery of anti-angiogenesis agents and other therapeutic molecules, Int. J. High Throughput Screen. 1 (2010) 171–181 2010.
[60] R.A. Cohen, T. Adachi, Nitric-oxide-induced vasodilatation: regulation by physiologic s-glutathiolation and pathologic oxidation of the sarcoplasmic endoplasmic reticulum calcium ATPase, Trends Cardiovasc. Med. 16 (4) (2006) 109–114.
[61] Y. You, A. Perkins, P. Cisternas, B. Munoz, X. Taylor, Y. You, H.J. Garringer, A.L. Oblak, B.K. Atwood, R. Vidal, C.A. Lasagna-Reeves, Tau as a mediator of neurotoxicity associated to cerebral amyloid angiopathy, Acta Neuropathol.Commun. 7 (1) (2019) 26.
[62] S. Utter, I.Y. Tamboli, J. Walter, A.R. Upadhaya, G. Birkenmeier, C.U. Pietrzik, E. Ghebremedhin, D.R. Thal, Cerebral small vessel disease-induced apolipoprotein E leakage is associated with Alzheimer disease and the accumulation of amyloid beta-protein in perivascular astrocytes, J. Neuropathol. Exp. Neurol. 67 (9) (2008) 842–856.
[63] R.A. Hill, L. Tong, P. Yuan, S. Murikinati, S. Gupta, J. Grutzendler, Regional blood flow in the normal and ischemic brain is controlled by arteriolar smooth muscle cell contractility and not by capillary pericytes, Neuron 87 (1) (2015) 95–110.